AIAA 2003–1235

Enhancement and Validation of PAB3D for Unsteady Aerodynamics

Steven J. Massey
Eagle Aeronautics, Inc., Hampton, VA 23669

Khaled S. Abdol-Hamid
Analytical Services & Materials, Inc., Hampton, VA 23666

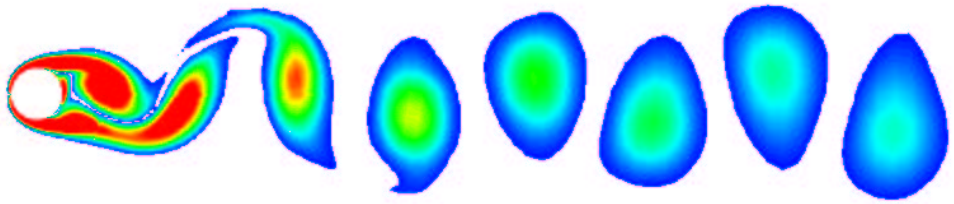

41st AIAA Aerospace Sciences Meeting and Exhibit
January 6–9, 2003/Reno, NV

Enhancement and Validation of PAB3D for Unsteady Aerodynamics

Steven J. Massey*
Eagle Aeronautics, Inc., Hampton, VA 23669
Khaled S. Abdol-Hamid†
Analytical Services & Materials, Inc., Hampton, VA 23666

The formulation, usage methodology and two validation examples are presented in support of the enhancement of PAB3D's time accurate capabilities. Two well known temporal integration schemes been added to provide second-order time accuracy by employing physical time sub-iteration and duel time sub-iteration. Comparisons with experimental data indicate both methods can be very accurate, but more study is needed to rigorously characterize the performance and accuracy of the schemes in PAB3D. Predictions of the Strouhal number of the Von Kármán vortex street for sample validation cases of low Reynolds number flow past a cylinder and high subsonic flow past a blunt flat plate, show good agreement with experimental data.

Introduction

Investigations in the area of unsteady flow control for propulsion applications have led to an increased interest in upgrading PAB3D's time accurate capabilities. PAB3D is a structured, multiblock, parallel, implicit, finite-volume solver, of the three-dimensional, unsteady, Reynolds-averaged Navier-Stokes equations. Advanced turbulence models are available and are widely used in internal and external flow applications by NASA and the US aerospace industry. In recognition of the importance of the continued enhancement of the PAB3D solver for use in industry and government projects, NASA Langley Research Center has advocated the long-term development of the code. The present addition of improved algorithms for second-order time accuracy, sub-iteration schemes and unsteady jet boundary conditions provide key modernizing enhancements to the code. In this task, two widely used time advancement schemes[1–3] are implemented in PAB3D and validated against experimental data.[4–6]

Time Advancement Formulation

The flux vector form of the Navier-Stokes equations may be written in indicial notation as

$$\frac{1}{J}\frac{\partial \mathbf{Q}}{\partial t} = -\frac{\partial}{\partial \xi_j}\left[\mathbf{E}_j - (\mathbf{E}_v)_j\right] = \mathbf{R}(\mathbf{Q}) \tag{1}$$

where $\mathbf{Q}$ is the flow vector, $\mathbf{E}_j$ and $(\mathbf{E}_v)_j$ are the j^{th} inviscid and viscous flux vectors respectively and $\mathbf{R}$ is the residual vector. The time dependent term may be discretized with backward differencing as

$$\frac{(1+\phi)(\mathbf{Q}^{n+1}-\mathbf{Q}^{n}) - \phi(\mathbf{Q}^{n}-\mathbf{Q}^{n-1})}{J\Delta t} = \mathbf{R}(\mathbf{Q}^{n+1}) \tag{2}$$

and rearranging Eq. (2) gives

$$\frac{(1+\phi)}{J\Delta t}(\mathbf{Q}^{n+1}-\mathbf{Q}^{n}) = \mathbf{R}(\mathbf{Q}^{n+1}) + \frac{\phi(\mathbf{Q}^{n}-\mathbf{Q}^{n-1})}{J\Delta t} \tag{3}$$

where the superscripts indicate the time level, and $\phi = 0$ and $\phi = \frac{1}{2}$ result in a first or second-order time accurate difference respectively. As a means of improving time accuracy, two sub-iteration schemes are implemented, duel or pseudo time stepping and physical time stepping. In duel time sub-iterations, the time step is allowed to vary across all cells based on a constant CFL. In physical time sub-iteration the time step is constant for all cells. For the duel time scheme, an additional pseudo time term is added to Eq. (2),

$$\frac{\mathbf{Q}^{m+1}-\mathbf{Q}^{m}}{J\Delta\tau} + \frac{(1+\phi)(\mathbf{Q}^{m+1}-\mathbf{Q}^{n})}{J\Delta t} = \mathbf{R}(\mathbf{Q}^{m+1}) + \frac{\phi(\mathbf{Q}^{n}-\mathbf{Q}^{n-1})}{J\Delta t} \tag{4}$$

and rearranging Eq. (4) gives

$$\left[\frac{1}{J\Delta\tau} + \frac{(1+\phi)}{J\Delta t}\right](\mathbf{Q}^{m+1}-\mathbf{Q}^{m}) = \mathbf{R}(\mathbf{Q}^{m+1}) + \frac{\phi(\mathbf{Q}^{n}-\mathbf{Q}^{n-1})}{J\Delta t} - \frac{(1+\phi)(\mathbf{Q}^{m}-\mathbf{Q}^{n})}{J\Delta t} \tag{5}$$

where m is the sub-iteration index and $\Delta\tau$ represents the pseudo time step. As $m \to \infty$, the pseudo term vanishes and with convergence $\mathbf{Q}^{m+1} \to \mathbf{Q}^{n+1}$. To generalize the time accurate scheme for any of the implicit formulations in PAB3D, $\mathbf{R}(\mathbf{Q})$ is linearized and

*Senior Research Scientist, AIAA Member.
†Senior Scientist, AIAA Associate.

the RHS is rewritten as,

$$RHS = \mathbf{R}(\mathbf{Q}^m) + \frac{\phi(\mathbf{Q}^n - \mathbf{Q}^{n-1})}{J\Delta t} - \frac{(1+\phi)(\mathbf{Q}^m - \mathbf{Q}^n)}{J\Delta t} \tag{6}$$

Additionally, the time step in the implicit side is replaced by

$$\frac{1}{J\Delta t_{imp}} = \left[\frac{1}{J\Delta\tau} + \frac{(1+\phi)}{J\Delta t}\right] \tag{7}$$

where the quantity $\Delta\tau$ is set according to a constant CFL number. The physical time sub-iteration scheme is similar to the duel time stepping method with the exception that the implicit time step term is now defined as

$$\frac{1}{J\Delta t_{imp}} = \left[\frac{(1+\phi)}{J\Delta t}\right] \tag{8}$$

Usage

The interface to the new time accurate features reside on a new segment of the `user.cont` file, an example and definitions are given as follows:

```
'Begin TimeStep Cont'
ir0  ratr ita cfltau ncycle
  1  0.10  -2     5.      5
'End TimeStep Cont'
```

Variable	Value	Definition
`ir0`	0*	Residual calculated from l_2 norm of $\mathbf{Q}$ over all cells
	1	Residual calculated from l_2 norm of ρ over all cells
`ratr`	0.5*	Limiter factor based on ρ per time step and imposed on $\mathbf{Q}$
`ita`	1*	First-order time accuracy with physical time sub-iteration
	2	Second-order time accuracy with physical time sub-iteration
	-1	First-order time accuracy with duel time sub-iteration
	-2	Second-order time accuracy with duel time sub-iteration
`cfltau`		CFL number for duel time sub-iteration
`ncycle`		Number of time iterations per physical time level, *e.g.* `ncycle`=1 for no sub-iterations. Typical value is 5, which gives 4 sub-iterations.

where (*) denotes the default value used when the `TimeStep` segment is omitted. The constant global time step is calculated from the CFL of the smallest cell, provided by the `dt` input in the `tpab3d.cont` file. Note, that `dt < 0` indicates the CFL per grid cell is constant for pseudo time stepping. To obtain the actual time step used for time accurate calculations, see the `PAB.out` file, for example:

```
Time Accurate Procedure
dtmin=   2.3720261E-08
dtmax=   4.9344753E-06
CFLM=    100.0000
time step in secs   2.3720261E-06
normalized time step    8.0963218E-04
Actual CFL =    100.0000
```

Results

Two geometries are examined to validate the time accuracy of the code, a circular cylinder and a flat plate with semicircular end caps. The flow about the cylinder is solved for low Reynolds number and low Mach. The flow about the plate is solved with a moderate Reynolds and high subsonic Mach. In both cases, the vortex shedding reduced frequency is compared with experimental results.

Circular Cylinder in Cross-flow

The frequency with which vortices are shed in a Kármàn vortex street behind a circular cylinder has been studied in numerous experiments,[4–6] from which an experimental range of dimensionless frequency or Strouhal number, St, is tabulated and plotted along with CFD results, see Table 1 and Figure 1. Strouhal number is defined as

$$St = \frac{nD}{V} \tag{9}$$

where n is the dimensional frequency, D is the cylinder diameter and V is the free-stream velocity.

Table 1 Circular Cylinder: Strouhal number results

Re_D	2nd-order duel	2nd-order physical	Experiment[4–6]
100	0.158	0.154	0.160-0.170
200	0.182	0.196	0.180-0.200
1000	0.198	0.225	0.195-0.215
10000	0.200	0.240	0.190-0.205

The flow field around the cylinder is simulated by solving the unsteady, compressible, laminar Navier-Stokes equations using an implicit, up-wind, flux-difference splitting, finite volume scheme. Turbulence is not modeled, due to the uncertain time accuracy of the models and the fact that the Reynolds numbers are well below the $Re_{crit} \approx 30,000$.[6] The 2D grid consisted of 34,832 cells and 6 blocks, and extended 20 diameters into the far-field, see Figure 2. The same grid was used for all runs, which gave a maximum y^+ range of approximately 0.04 to 17. The diameter of the cylinder, D was at $Re = 200$ was 0.235 mm and the Mach number for all cylinder cases was $M = 0.3$. The shedding frequencies are observed from the pressure contribution of lift, which is obtained via the internal *Post* stream thrust function integrated over the solid

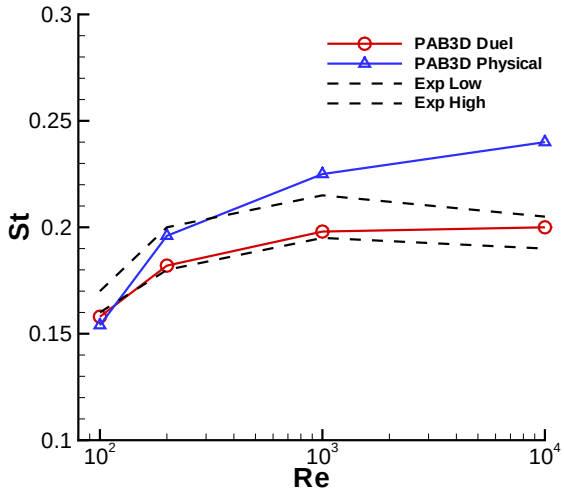

Fig. 1 Circular Cylinder: Strouhal number CFD results compared with experimental range.[4–6]

surface, which is equivalent to integrating surface pressure. Sample contour plots at of Mach number and vorticity magnitude at $Re = 200$ illustrate the vortex street formation, see Figures 3 and 4.

The solution strategy for this case is to first run at coarse grid level and large time step to trigger the asymmetric vortex shedding instability, then refine the grid and time step for accuracy. Sample plots for $Re = 200$ of C_L history for four time integration schemes are shown in Figures 5- 8, where

$$C_L = \frac{L}{\frac{1}{2}\rho V^2 S} \tag{10}$$

and S is area of the cylinder section solved. In each plot the onset on asymmetric vortex shedding is seen to occur just after 10^{-4} seconds and the switch to fine grid is seen to coincide with a increase in amplitude of C_L at 4×10^{-4} seconds. Confidence in the final solution is enhanced by the fact that the fine grid amplitudes for both second-order with sub-iteration methods are the same, while the coarse grid solutions vary widely. For the second-order time accurate cases, it was observed that approximately five time iterations per physical time step produced the optimal convergence per iteration. However, the physics of the specific problem will dictate this number for other cases. In the present results, five iterations typically reduced the residual by three orders of magnitude at that time level, with no improvement for more iterations. Thus, it is concluded that the final solutions are converged in time and space. However, to definitively characterize the temporal and spacial convergence more study of each flow condition and further grid refinement is required.

As a benchmark against previous versions of PAB3D, results for the first order time accurate integration scheme with no sub-iterations were included

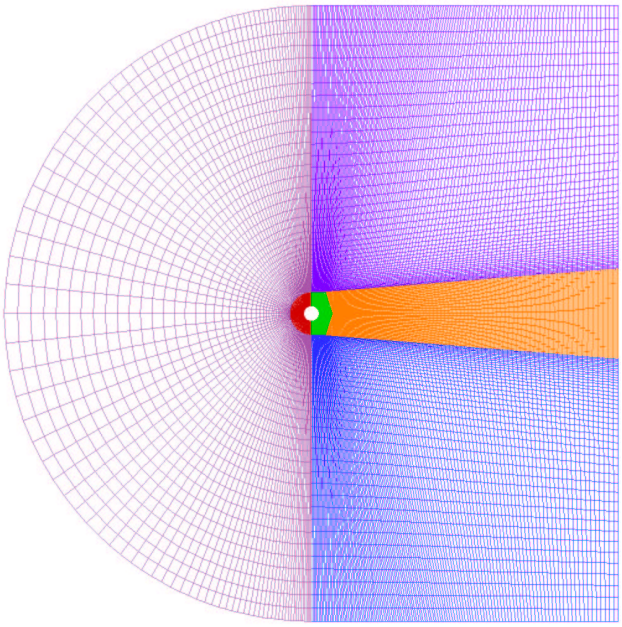

a) Full Domain.

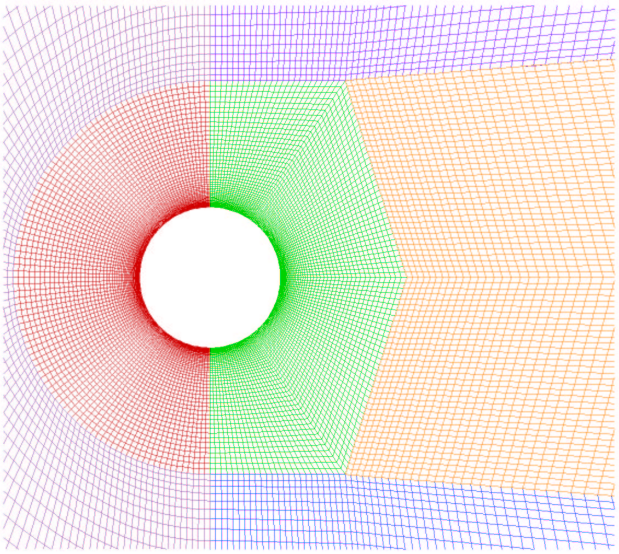

b) Close up.

Fig. 2 Circular Cylinder: Grid colored by block.

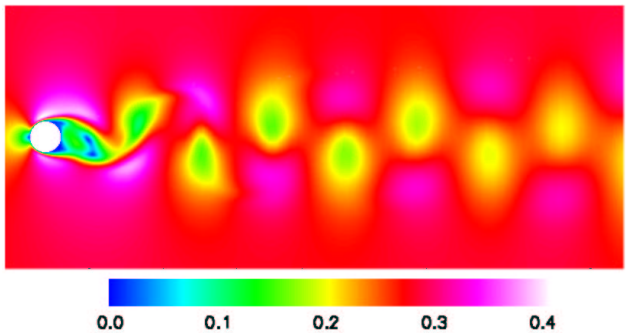

Fig. 3 Circular Cylinder, $Re = 200$: Mach contours, second-order, duel time solution.

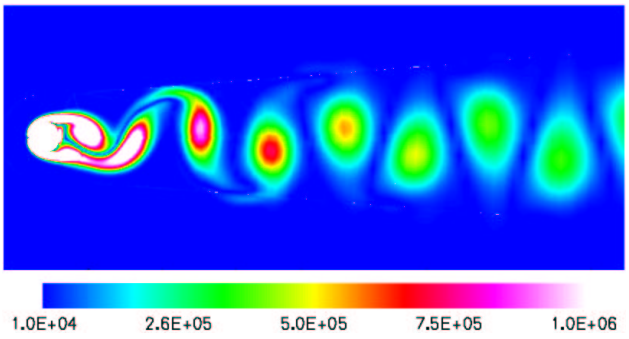

Fig. 4 Circular Cylinder, $Re = 200$: Vorticity magnitude contours $[1/s]$, second-order, duel time solution.

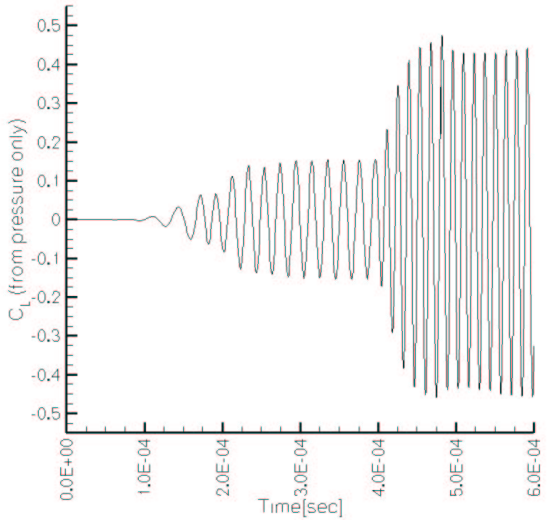

Fig. 5 Circular Cylinder, $Re = 200$: C_L history, 1st-order time accurate, no sub-iteration.

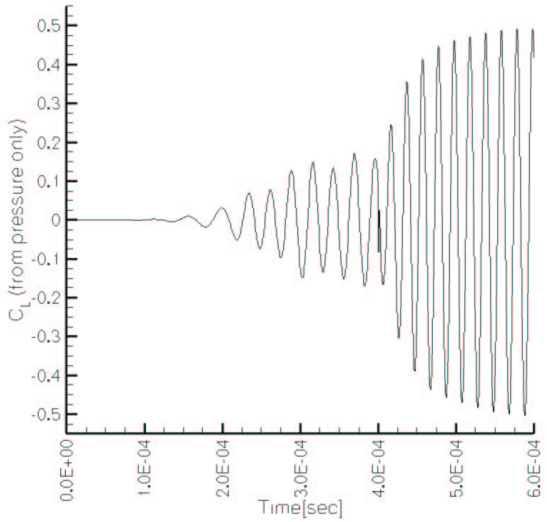

Fig. 6 Circular Cylinder, $Re = 200$: C_L history, second-order time accurate scheme, no sub-iteration.

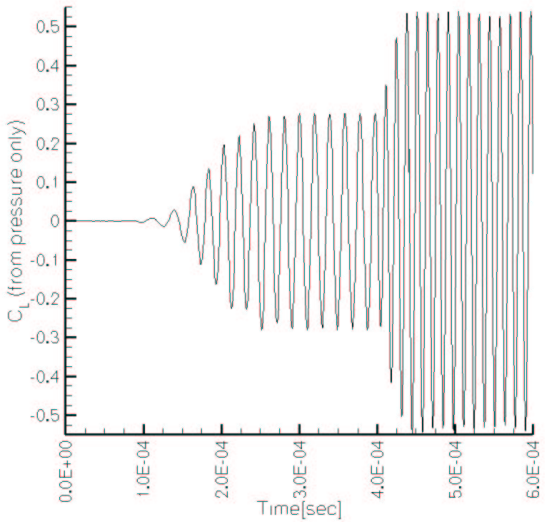

Fig. 7 Circular Cylinder, $Re = 200$: C_L history, second-order time accurate, with five duel time iterations.

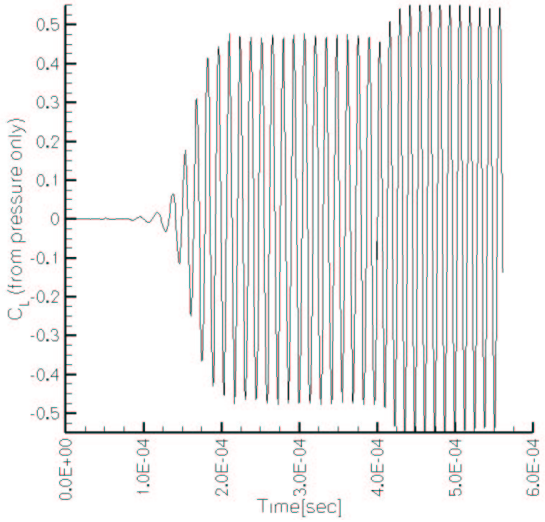

Fig. 8 Circular Cylinder, $Re = 200$: C_L history, second-order time accurate, with physical time iterations.

for the $Re = 200$ case, Figure 5, which corresponded to a reduced frequency of $St = 0.175$. Also included, are the results for the second order scheme with no sub-iterations at $Re = 200$, Figure 6, which gives a reduced frequency of $St = 0.159$. The second order scheme with no sub-iterations is seen to be more less accurate than the first order scheme. This is a result of the second order scheme being only second order accurate within the sub-iterations. Thus, sub-iterations are *required* for both second order schemes described in the paper.

The physical time iteration scheme, showed the most consistent amplitude and frequency for C_L between coarse and fine solutions for $Re = 200$. However, for

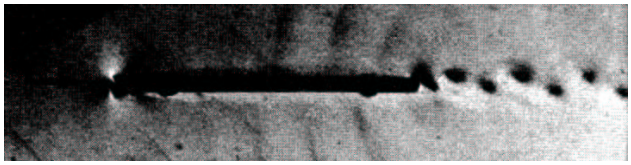

Fig. 9 Flat Plate: Schlieren image of Von Kármán vortex street behind a flat plate at zero incidence ($M = 0.61$, $Re = 6.5 \times 10^5$, $D/l = 0.05$, $l = 60$ mm). From Schichting[6] after Heinemann *et al.*[7]

higher Re the physical time scheme consistently over predicted the shedding frequency, while the duel time scheme stayed within experimental bounds.

Flat Plate at Zero Incidence

Since PAB3D is a compressible code, it is desirable to assess its time accuracy in a compressible flow. In this case, the computed vortex shedding frequency from behind a slender flat plate at zero incidence with Mach number between $0.3 < M_\infty < 0.8$ is compared with the experimental results from Heinemann *et al.*,[7] see Figure 9. As in the cylinder case, the flow is also laminar, and thus is solved as such. The assessment of PAB3D's various turbulence models for unsteady flows is an ongoing topic and is beyond the scope of the present study, which will serve as a basis for future studies.

The 2D grid for the plate was generated by modifying the existing cylinder grid by extending the boundary to 40 diameters and adding the flat middle section. To enable the case to run efficiently in parallel, the grid is divided into 15 blocks totaling 68,000 cells, see Figure 10. The same grid was used for all runs, which gave a maximum y^+ range of approximately 1.5 to 2.0 at the trailing edge. The plate length including end caps is $l = 60$ mm and the ratio of diameter to length is $D/l = 0.03$. In both the cylinder and plate cases only one cell was used in the 2D direction. In practice, adding at least one more cell in the thickness direction often enhances convergence.

The flow field for the plate is similar to the cylinder, the exception being that the plate boundary layer is seen to separate in two locations. Mach number, simulated Schlieren and vorticity magnitude contours for an example condition of $M = 0.61$ clearly show the fore and aft separation and vortex shedding pattern, see Figures 11- 13. In view of the forward separation and the expected weak variation of lift, only a partial integration of pressure for drag was done along the top half of the trailing edge of the plate. Since, only the frequency of the vortex street is desired, the actual drag or lift is not needed. A close up view of the shedding structure at the trailing edge is shown in Figure 14. Unlike the low Re cylinder case, a complex arrangement of smaller vortices are observed at the trailing edge which then merge into larger more regular vortices making up the street. The additional

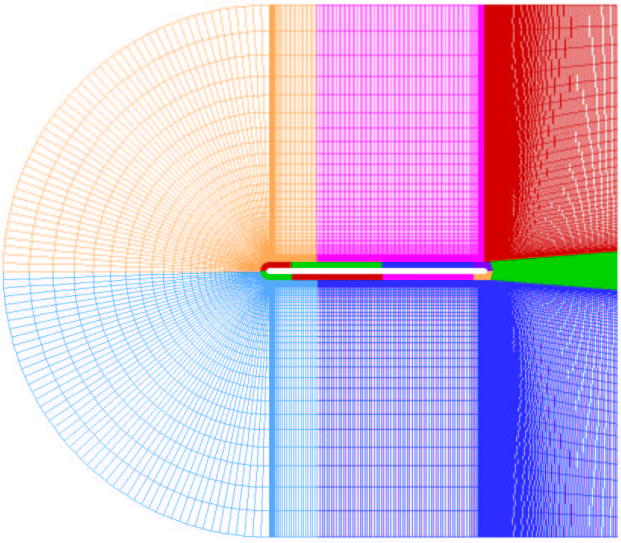

a) Full Domain.

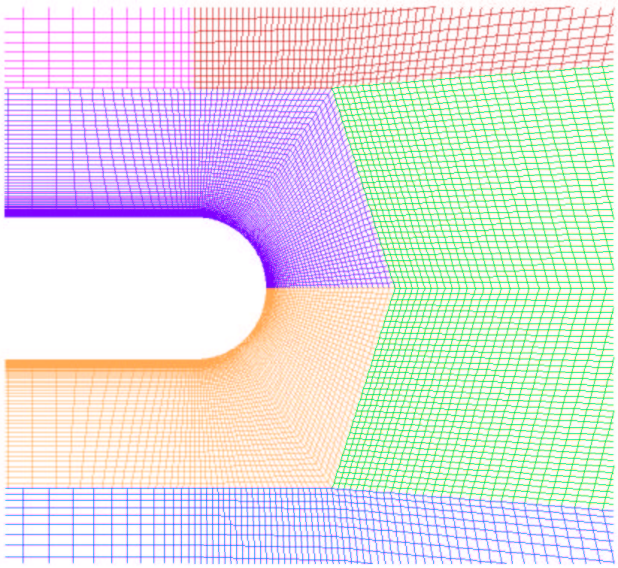

b) Trailing Edge.

Fig. 10 Flat Plate: Grid colored by block.

vortices close to the surface are also seen to increase the fluctuation of the partial drag force histories, see Figures 15 and 16. The fluctuation is also seen to be the greatest after $t = 7 \times 10^4$ sec, which is when the grid and time step were refined. This is likely due to the increased fidelity of the modeling of the secondary trailing edge separations.

By taking an average of at least 6 cycles, reduced frequencies were tabulated and plotted with experimental results of Heinemann *et al.*[7] for a wide range of subsonic Mach and laminar Reynolds number, see Table 2 and Figure 17. Results are seen to be in fair agreement and improve to within 4% as Mach number increases. A possible cause is a lack of convergence. This case was set up at the condition of $M = 0.61$ and the other conditions were run with the same ex-

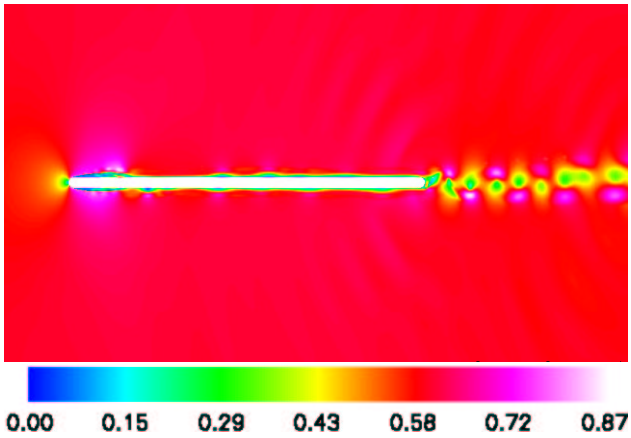

a) Mach number, M.

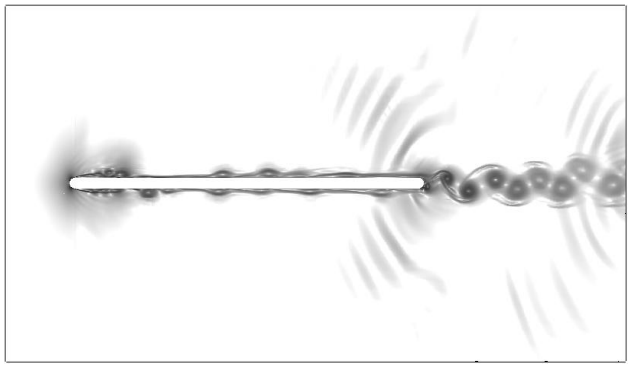

b) Simulated Schlieren, $ln||\nabla\rho||$.

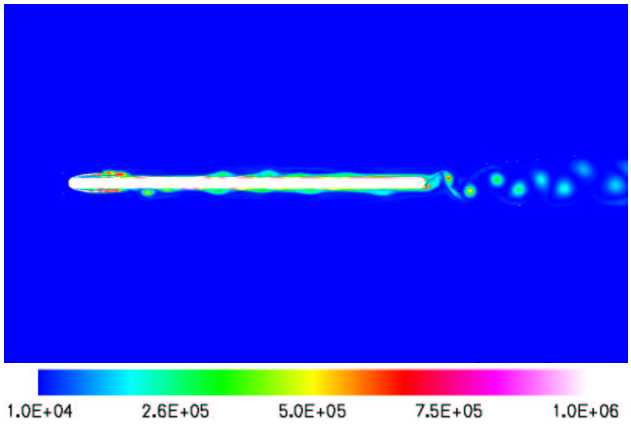

c) Vorticity magnitude, $||\omega||$ $[1/s]$

Fig. 11 Flat Plate, $M = 0.61$: Full plate view.

act time step and number iterations. It is likely, that with more sub-iterations and or a smaller time step the accuracy will improve.

Concluding Remarks

PAB3D's time accurate capabilities have been successfully upgraded to second-order time accuracy using two proven approaches, physical time sub-iteration and duel time sub-iteration. Comparisons with experimental data indicate both methods can be very accurate, but more study is needed to quantify the error

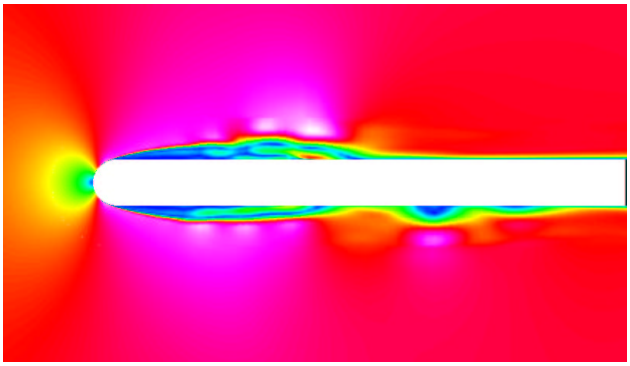

a) Mach number, M.

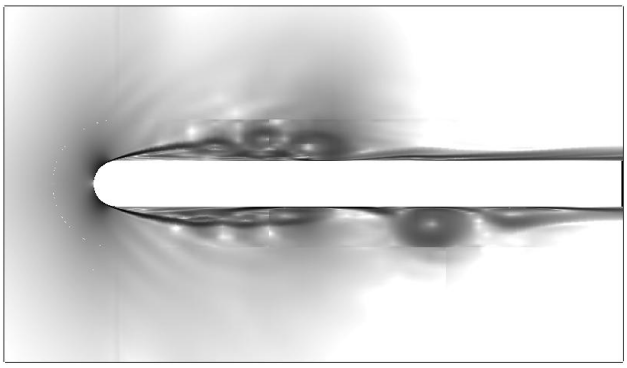

b) Simulated Schlieren, $ln||\nabla\rho||$.

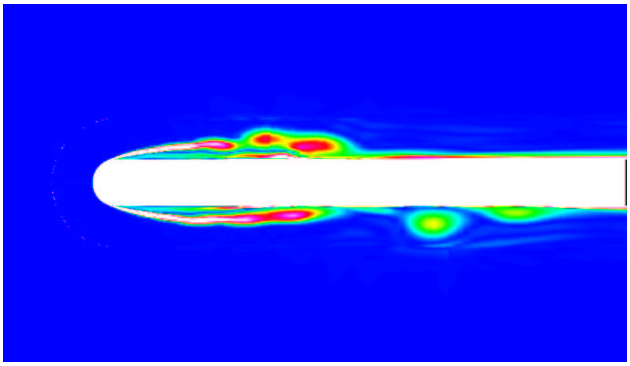

c) Vorticity magnitude, $||\omega||$ $[1/s]$

Fig. 12 Flat Plate, $M = 0.61$: Leading edge view.

Table 2 Flat Plate: Strouhal number results for $D/l = 0.03$

M_∞	$Re_l[10^5]$	2nd order duel	2nd order physical	Exp.[7]
0.30	4.0	0.255	0.247	0.197
0.43	5.3	0.246	0.243	0.196
0.55	6.2	0.226	0.219	0.193
0.61	6.5	0.211	0.207	0.189
0.69	7.3	0.192	0.191	0.184
0.80	7.5	0.190	0.184	0.178

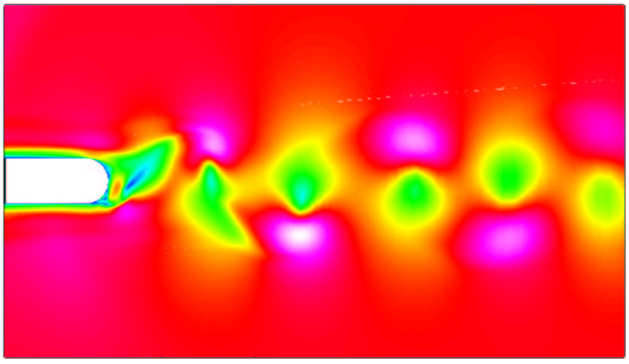

a) Mach number, M.

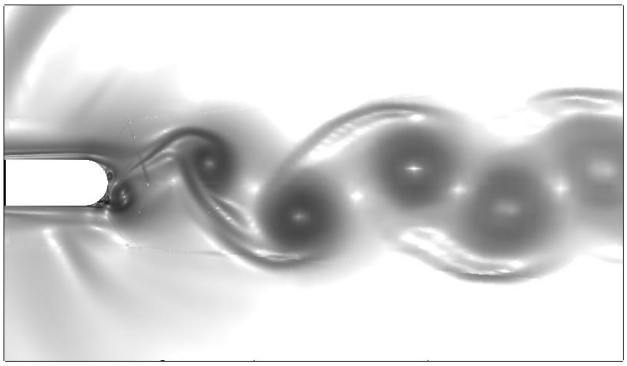

b) Simulated Schlieren, $ln||\nabla\rho||$.

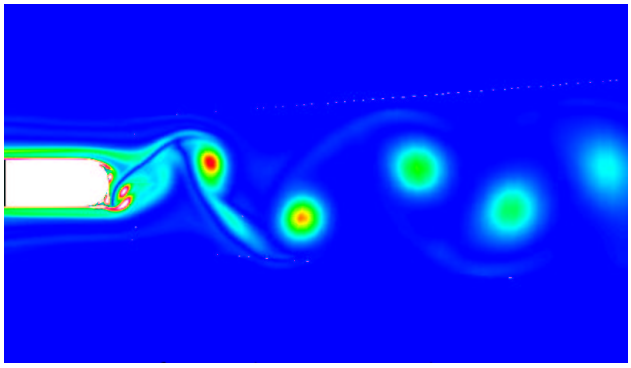

c) Vorticity magnitude, $||\omega||$ $[1/s]$

Fig. 13 Flat Plate, $M = 0.61$: Trailing edge view.

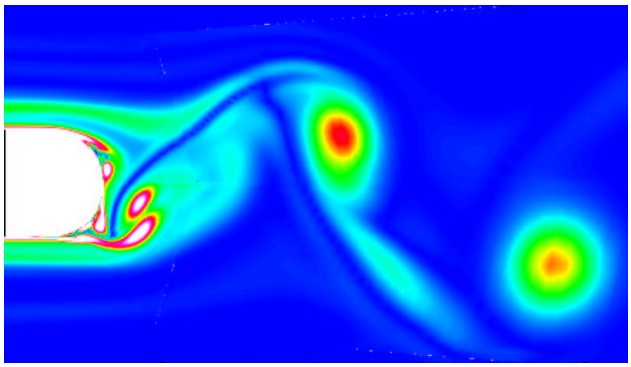

Fig. 14 Flat Plate, $M = 0.61$: Close up view showing of vorticity magnitude showing multiple levels of vortex shedding.

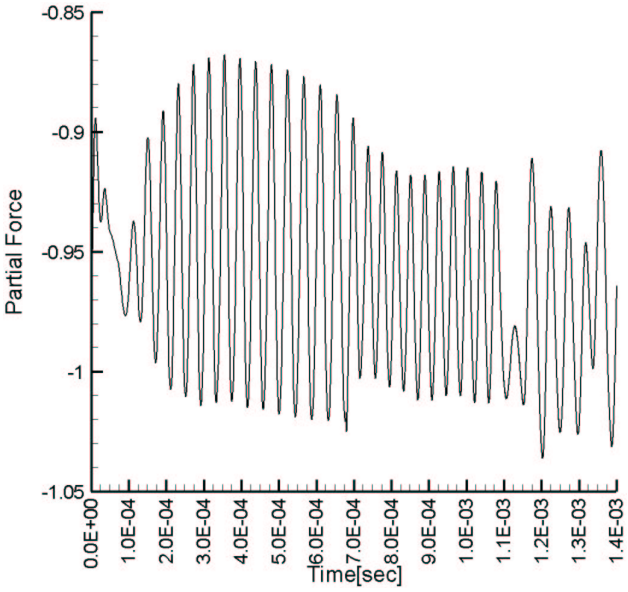

Fig. 15 Flat Plate, $M = 0.61$: Upper trailing edge pressure history, second-order time accurate, with five duel time iterations.

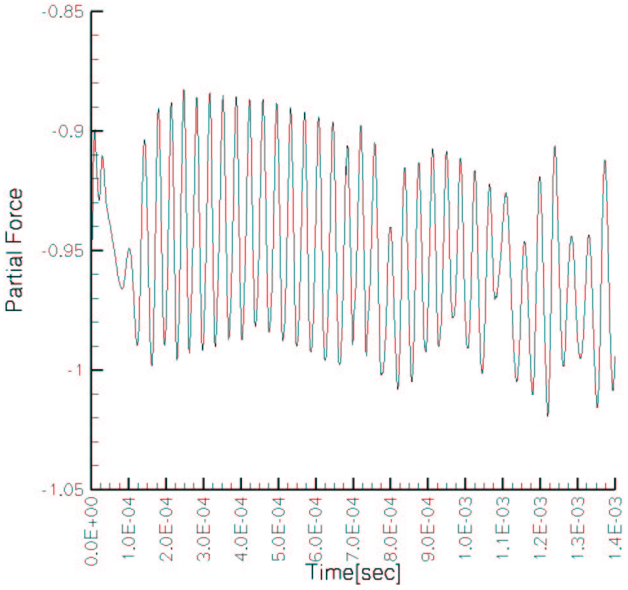

Fig. 16 Flat Plate, $M = 0.61$: Upper trailing edge pressure history, second-order time accurate, with five physical time iterations.

observed in some of the solutions. It should be noted that for an equal sized time step and number of iterations per time level, the physical time iteration scheme will always have less error than the duel time scheme. The purpose of duel time stepping is to enable the use of a larger time step than would normally be allowed by stability. Thus, the real advantage of duel time stepping is for convergence acceleration. As a baseline, in this study the time step and number of iterations were held constant for each scheme and flow condition. Further investigation is required to determine the optimal PAB3D parameters and methodology to obtain

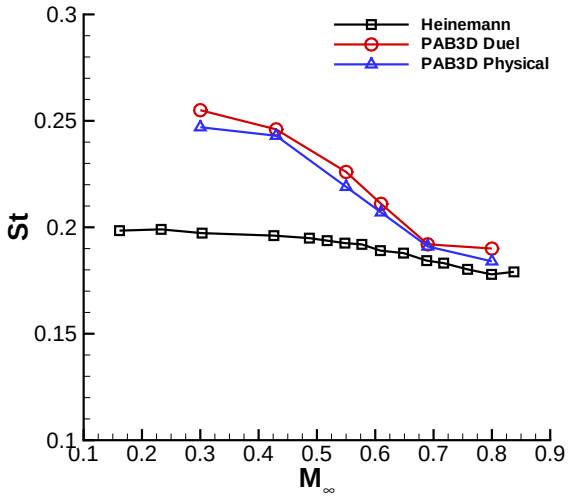

Fig. 17 Flat Plate: Strouhal number results.

the most accurate and efficient solutions.

Acknowledgments

The authors wish to thank Craig Hunter and Karen Deere of the Configuration Aerodynamics Branch of NASA Langley Research Center for their helpful input and for the contribution of the cylinder grid.

References

[1]Pulliam, T., "Time Accuracy and the Use of Implicit Methods," AIAA Paper 93-3360, 1993.

[2]Jameson, A., "Time Dependent Calculations Using Multigrid with Applications to Unsteady Flows Past Airfoils and Wings," AIAA Paper 91-1595, 1991.

[3]Rumsey, C., Sanetrick, M., Biedron, R., Melson, D., and Parlette, E., "Efficiency and Accuracy of Time-Accurate Turbulent Navier-Stokes Computations," AIAA Paper 95-1835, 1995.

[4]Morkovin, M., "Flow Around a Circular Cylinder - A Kaleidoscope of Challenging Fluid Phenomena," 1964, In proceedings of ASME Symposium on Fully Separated Flows.

[5]Roshko, A., "Experimental on Flow Past a Circular Cylinder at Very High Reynolds Number," *Journal of Fluid Mechanics*, Vol. 10, No. 2, 1961, pp. 345–356.

[6]Schlichting, H., *Boundary-Layer Theory*, McGraw-Hill, New York, 1979.

[7]Heinemann, H., Lawaczeck, O., and Bütefisch, K., "Kármàn vortices and their frequency determination in the wakes of profiles in the sub- and transonic regime," Symposium Transsonicum II Göttingen. Springer Verlag pp. 75-82., 1976.